JOURNAL OF SYNCHROTRON RADIATION
ISSN 1600-5775

Compact IR synchrotron beamline design

Thierry Moreno*

Optics Group, Synchrotron SOLEIL, L'Orme des Merisiers, Saint-Aubin, BP 48, 91192 Gif sur Yvette Cedex, France.
*Correspondence e-mail: thierry.moreno@synchrotron-soleil.fr

Received 3 October 2016
Accepted 26 December 2016

Edited by M. Eriksson, Lund University, Sweden

Keywords: infrared synchrotron beamline; multi-bend achromat storage ring; bending-magnet source; optical aberrations; integrating magnetic and photonic synchrotron beamline components.

Third-generation storage rings are massively evolving due to the very compact nature of the multi-bend achromat (MBA) lattice which allows amazing decreases of the horizontal electron beam emittance, but leaves very little place for infrared (IR) extraction mirrors to be placed, thus prohibiting traditional IR beamlines. In order to circumvent this apparent restriction, an optimized optical layout directly integrated inside a SOLEIL synchrotron dipole chamber that delivers intense and almost aberration-free beams in the near- to mid-IR domain (1–30 µm) is proposed and analyzed, and which can be integrated into space-restricted MBA rings. Since the optics and chamber are interdependent, the feasibility of this approach depends on a large part on the technical ability to assemble mechanically the optics inside the dipole chamber and control their resulting stability and thermo-mechanical deformation. Acquiring this expertise should allow dipole chambers to provide almost aberration-free IR synchrotron sources on current and 'ultimate' MBA storage rings.

1. Introduction

Infrared (IR) radiation delivered by bending-magnet (BM) sources (Duncan & Williams, 1983; Schweizer *et al.*, 1985) is used at numerous synchrotron radiation facilities worldwide, notably to provide chemical two-dimensional analysis of molecular compounds with micrometric (Carr *et al.*, 1998; Dumas & Tobin, 2003; Dumas *et al.*, 2004) or nanometric resolution (Schnell *et al.*, 2009). This radiation is orders of magnitude brighter than conventional IR sources and is highly transversely coherent which perfectly matches the IR techniques of absorption spectroscopy.

In classical IR synchrotron beamlines, the first optic is almost always a plane mirror, reflecting either sidewards or upwards, whilst transmitting the less divergent X-rays through a slot in the mirror and thus avoiding mirror thermal deformation. In order to increase the photon beam intensity, the slotted mirror is placed as close as possible to the source, usually at the exit of the BM chamber, but the lack of space limits the mirror size and the horizontal beamline aperture to values not exceeding 80 mrad (Dumas *et al.*, 2006).

Nevertheless, new and already existing third-generation storage rings are currently evolving to the very compact multi-bend achromat (MBA) lattice (Eriksson *et al.*, 2008) which allows the horizontal emittance to reach well into the sub-nanometre radian region, delivering diffraction-limited X-ray beams at several keV, but leaves very little room for IR extraction mirrors to be placed, thus apparently condemning traditional IR beamlines to this category of rings. Thankfully, we have found a solution to this problem which integrates the IR front-end optics directly inside the dipole chamber. This proposal takes into account that the optics, fabricated in aluminium, are vacuum compatible with the dipole chamber

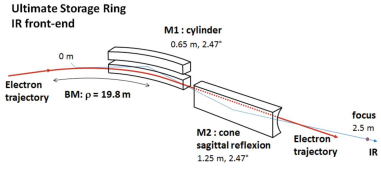

(which is also composed of aluminium or stainless steel) and that their closeness to the electron trajectory allows the collection of almost all the vertical BM emission in the near- to mid-IR domain, in spite of the small vertical size of the dipole chamber (1 to 2 cm), and has a limited impact on the impedance of the lattice. In addition, it is crucial that the mechanical accuracies of manufacture and alignment of the dipole chamber are compatible with the optical tolerances of the IR front-end, and this will be proven in §3. Since the optics and chamber are interdependent, the feasibility of this approach depends on a large part upon the technical ability to assemble mechanically the optics inside the dipole chamber and control their resulting stability and thermo-mechanical deformation.

A similar approach has already been successfully applied in the IR and terahertz domain (Kimura *et al.*, 2001, 2012) by using a magic mirror (López-Delgado & Szwarc, 1976) inside a dipole chamber. Nevertheless, the complex shape of this single mirror, which focuses conjointly the horizontal and vertical BM emission, demands a very precise mirror positioning. This is hardly compatible with the present mechanical accuracies of manufacture and alignment of the dipole chambers and requires, contrary to the method presented in this paper, the chamber supporting the mirror to be motorized.

In the following sections, the IR front-end optics and their integration inside the dipole chamber are described and analyzed (§2), and an example using a SOLEIL dipole chamber is given that shows the feasibility of the presented approach and which can be implemented in MBA lattices (§3).

In this study, only the synchrotron radiation mode of IR emission is considered but, since our optical layout removes the aberrations from all positions along the electron trajectory, in particular at the entrance of the BM, it also suits very well the edge radiation mode (Bosch *et al.*, 1996; Roy *et al.*, 2000). Although IR synchrotron radiation is almost fully transversally coherent, optical beam properties can be accurately described using a ray-tracing approach (Moreno & Idir, 2001) without reverting to a full wave-propagation calculation (Chubar & Elleaume, 1998). Besides, ray tracing is currently indispensable in order to properly evaluate the geometrical aberrations produced by the circular BM source trajectory and mirror profiles.

2. Method

The IR front-end layout consists of two aluminium mirrors, with cylindrical and cone-shaped profiles focusing separately the horizontal and vertical source emissions, respectively (Kirkpatrick & Baez, 1948), and optimized to remove the geometrical aberrations of the BM source (Moreno, 2015, 2016). These two mirrors are mechanically fixed into the dipole chamber and focus the beam at the end of the chamber. Figs. 1, 2 and 3 show the top-view scheme, a transversal cut of the chamber and the front-end optical layout, respectively. The cylindrical mirror follows the electron trajectory and horizontally focuses the IR radiation emitted by the BM towards the ring (Figs. 1–3). The cone-shaped mirror, facing towards the electron trajectory, focuses the vertical IR emission of the dipole upwards and towards the IR beamline. After this second mirror, the beam is almost aberration-free and can be redirected using simple plane mirrors toward the vacuum window, the focal plane and the collimating stage of the IR beamline. As these two mirrors are placed at very short distances from the source, their vertical acceptance is almost total in the near- to mid-IR domain (1–30 μm), despite the small vertical size of the chamber. Horizontally, the beamline aperture is given by the length of the cylindrical mirror which can theoretically cover the full dipole emission. Nevertheless, its aperture must be shortened both upstream, in order to avoid thermal deformations resulting from the radiation emitted by the upstream dipole and a possible upstream insertion device, and downstream, to prevent impedance instabilities by keeping the mirror edge at a safe distance from the electron trajectory (Nagaoka, 2004). Also, its positioning must remain compatible with the water-cooling elements contained inside the vessel: the crotch defining the straight section aperture (Fig. 1), the longitudinal absorber located on the sextupole and quadrupole magnets and the water-cooled slot separating the electron beam channel and the antechamber of the dipole vessel (Fig. 2). As in traditional IR beamline designs, the cylindrical mirror requires a horizontal slot (Fig. 2) along its whole length which allows the less divergent higher-energy X-rays to pass through thus almost eliminating thermal deformations.

Concerning the fixation of the mirrors, the current SOLEIL dipole chambers are machined from stainless steel sheets and made into two half-shells that are brazed in the medium plane

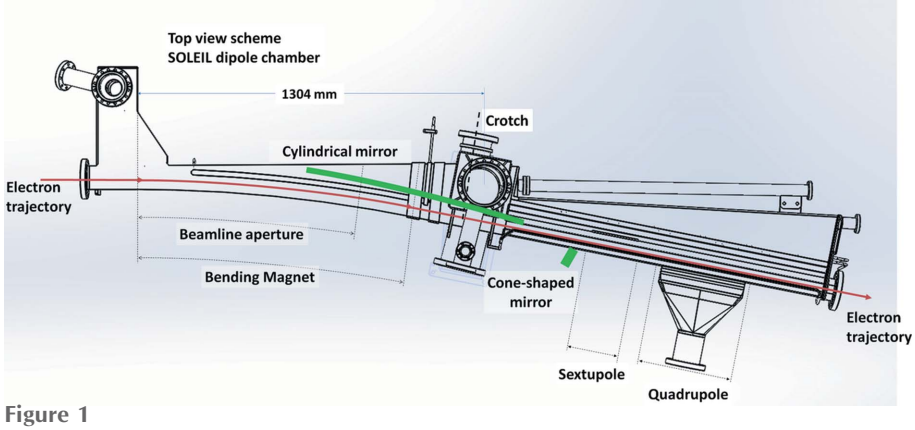

Figure 1
Top-view scheme of the SOLEIL BM vacuum chamber and the IR extraction system that comprises a cylindrical and cone-shaped mirror (in green). The cylindrical mirror focuses horizontally the light emitted by the source (edge radiation and synchrotron radiation) and follows almost in the same way the electron beam trajectory allowing an extremely large horizontal extraction (150 mrad), whereas the cone-shaped mirror, facing towards the electron trajectory, focuses the vertical BM IR emission in an upwards reflecting geometry. This extraction layout delivers an almost aberration-free IR beam that is focused at the vicinity of the chamber. To avoid thermal deformations, the cylindrical mirror is slotted (see Fig. 2) along its whole length, thus allowing X-rays to pass through.

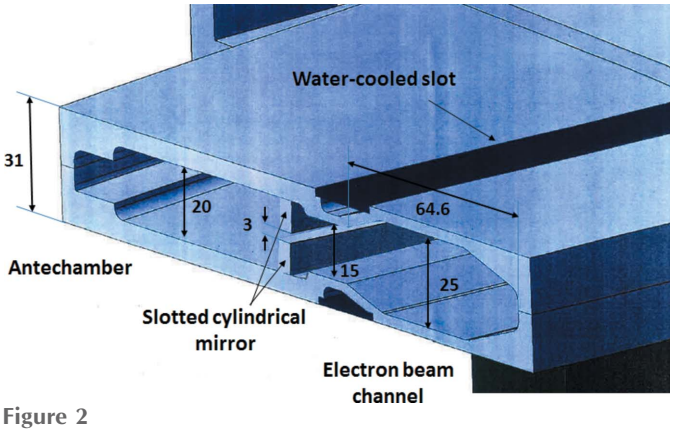

Figure 2
Cross section of a current SOLEIL vacuum dipole chamber at the end of the beamline aperture (Fig. 1), where distances are given in millimetres. The drawing shows the electron beam channel, the water-cooled slot device, the cylindrical mirror slotted in two parts to allow X-rays to pass through, thus eliminating thermal deformations, and the antechamber (which is used for vacuum pumping). The mirror, made of aluminium, is directly brazed onto the two parts of the stainless steel dipole chamber before assembling. Future SOLEIL dipole chambers could be manufactured from extruded aluminium profiles and the mirror would have to be maintained with supports inserted from the antechamber side ports.

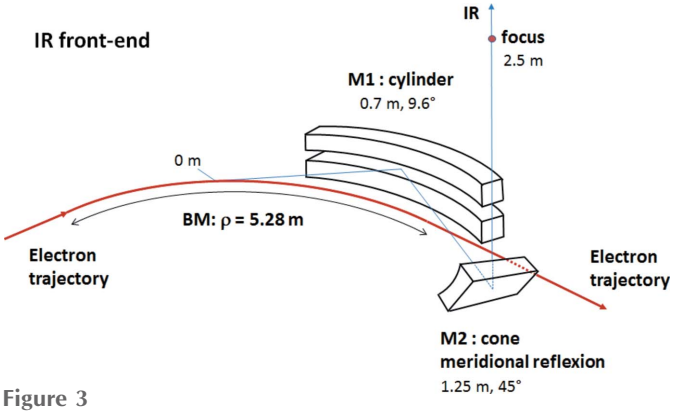

Figure 3
Optical scheme of the SOLEIL IR front-end example. The mirror positions are given according to optical path distances from the source.

to guarantee their very tight tolerances of planarity (±0.5 mm over the 2.5 m dipole chamber length) (Herbeaux, 2016). For this category of chambers, the cylindrical and the cone-shaped mirrors can be directly brazed on each half-shell before final assembling. In the future, an upgraded SOLEIL dipole chamber could be manufactured from extruded aluminium profiles, and the cylindrical and cone-shaped mirrors would have to be maintained with supports inserted from the antechamber and beam channel side ports, respectively.

It is important to stress that for very space-restricted MBA lattices such as found at MAX IV (Eriksson *et al.*, 2011) a more suitable mirror arrangement can be obtained by designing the cone-shaped mirror for sagittal focusing (instead of meridional focusing as treated in §3). Fig. 4 shows a possible arrangement for the MAX IV lattice, where an almost free-aberrated optical solution can be obtained by focusing the beam at 2.5 m from the source with mirror grazing angles of 2.47°. In this geometry, both mirrors are facing each other and

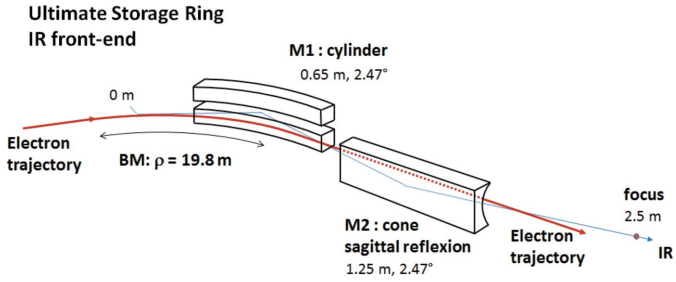

Figure 4
Possible optical arrangements for a 'MAX IV type' MBA lattice, where the cone-shaped mirror is used in sagittal focusing [equation (5)]. An almost free-aberrated optical solution can be obtained by focusing the beam at 2.5 m from the source with mirror grazing angles of 2.47°. This optical configuration allows having the two mirrors facing each other and almost parallel to the dipole chamber, while limiting impedance instabilities. Equations (1), (2), (3) and (5) give the best position and radius of the two mirrors: $p = 650$ mm and $R = 22.322$ m for the cylindrical mirror, and for the cone-shaped mirror $p = 1250$ mm and $r(x) = r_0(1 + ax)$ with $r_0 = 53.87$ mm and $a = -2.21 \times 10^{-5}$ mm^{-1}. Due to the small mirror grazing angle, the conical term 'a' is negligible.

are almost aligned to the 25 mm-diameter electron beam channel whilst reflecting the beam in the ring orbit plane. This optical configuration would allow the mirrors to be placed at least partially inside the dipole chamber, while keeping acceptable impedance levels, but the aperture of the quadrupoles and sextupoles surrounding the mirrors must certainly be modified accordingly. In addition, a third plane mirror has to be used in order to deflect transversely the IR beam before reaching the dipole source of the following MBA cell magnet block.

2.1. Optimization of the optical layout

The main parameters of the two mirrors, such as their positions inside the chamber, orientations and radii of curvature, are determined in order to minimize beam aberrations generated by the BM source. An optical path method is used (Noda *et al.*, 1974; Howells, 1992) which is summarized below for the horizontal and the vertical directions, respectively.

Horizontally, equations (1), (2) and (3) provide the optical parameters of the cylindrical mirror in order to remove defocus, coma and spherical beam aberrations, respectively, which are generated by the circular shape of the BM source trajectory,

$$\frac{1}{p}+\frac{1}{q}=\frac{2}{R\sin(\theta)}, \tag{1}$$

$$\frac{p}{q}=\left[1-\frac{2\rho\tan(\theta)}{3p}\right]^{1/2}, \tag{2}$$

$$\frac{p}{q}\left(\frac{3p}{q}-1\right)^2=\tan^2(\theta)\left(1-\frac{p}{q}\right)^2, \tag{3}$$

where p, q, R and θ are the source and image distances of the cylindrical mirror, its radius of curvature and the grazing

angle, respectively, and ρ is the radius of curvature of the BM source.

In the vertical direction, a cone-shaped mirror is used to correct for vertical BM aberrations. Equations (4) and (5) give, for the cone-shaped mirror in meridional and sagittal focusing, respectively, the local radius of curvature of this mirror as a function of the position x along its axis,

$$R(x) = \frac{2pq}{\sin(\theta)(p+q)}\left[1 - \frac{M_{\rm H}}{(L_{\rm H}-p)}\frac{q\rho}{p(p+q)}x + \ldots\right], \quad (4)$$

$$r(x) = \frac{2pq\sin(\theta)}{(p+q)}\left(1 - \left\{\left[\frac{1}{(L_{\rm H}-p)} + \frac{1}{p} - \frac{1}{q}\right]\cos(\theta) - \frac{M_{\rm H}}{(L_{\rm H}-p)}\frac{q\rho}{p(p+q)}\sin(\theta)\right\}x + \ldots\right), \quad (5)$$

where p, q and θ are the source and image distances of the cone-shaped mirror and its grazing angle, respectively, and ρ is the radius of curvature of the BM source. $M_{\rm H}$ and $L_{\rm H}$ are the horizontal magnification and the source-to-image distance of the cylindrical mirror when this mirror is placed in between the source and the cone-shaped mirror. $M_{\rm H} = -1$ and $L_{\rm H} = 0$ otherwise.

The vertical coma aberration is removed by using equal image and source distances.

This layout has already been successfully demonstrated for a traditional IR synchrotron beamline (Moreno *et al.*, 2013).

3. Application

The method described above is now applied to a SOLEIL dipole chamber (Figs. 1 and 2). Table 1 provides the electronic parameters of the SOLEIL BM source. Fig. 3 and Table 2 give the main optical parameters of the IR front-end example, where mirror positions are given as optical path distances from the source. The front-end is optimized to collect horizontally 150 mrad of the BM IR emission (edge radiation and synchrotron radiation), which represents 80% of the dipole aperture. In order to provide an aberration-free beam from such a large aperture, source aberrations must be removed up to and including the spherical terms [equation (3)] for the cylindrical mirror. A good choice for this SOLEIL configuration is to place the focal plane at 2.5 m from the source and equations (1)–(3) allow the grazing angle and position of the cylindrical mirror to be determined at $\theta = 9.6^\circ$ and $p = 700$ mm, respectively. The vertical beamline aperture is then limited to 21 mrad (mid-IR) by the chamber height in between the beam channel and the antechamber (15 mm). The cone-shaped mirror is used in meridional reflection [equation (4)] and it is placed mid-way between the source and the focal plane ($p = q = 1.25$ m) in order to remove vertical coma aberrations of the source. With a grazing angle of 45° (reflecting upwards), the local radius of curvature for the best cone-shaped profile as a function of position (x) along the mirror length, $R(x) = R_0(1 + ax + bx^2)$ is obtained with $R_0 = 17.678$ m, $a = 4.328 \times 10^{-3}$ mm^{-1} and $b = 1.839 \times 10^{-5}$ mm^{-2}.

Table 1
Main parameters of the SOLEIL machine and BM source.

Electron energy, current	$E_0 = 2.739$ GeV, $I_0 = 0.5$ A
Bending magnet	$B = 1.71$ T, $\rho = 5.28$ m
Electron beam size	$\sigma_{eX} \times \sigma_{eZ} = 63.1$ µm × 32.4 µm RMS (H × V)
Electron beam divergence	$\sigma'_{eX} \times \sigma'_{eZ} = 135$ µrad × 2 µrad RMS (H × V)

Table 2
Parameters of the IR front-end layout.

Element	Optical path distances	Geometry	Footprint @ 99%, λ = 30 µm, length × width
Diaphragm	0 m	150 mrad × 21 mrad (H × V)	
M1 mirror	0.7 m	Cylinder, horizontal focusing, $\theta = 9.6^\circ$, sideward	772 mm × 15 mm
M2 mirror	1.25 m	Cone-shaped, vertical focusing, $\Delta R/R = \pm 18.8\%$ over ±34 mm, $\theta = 45^\circ$, upward	44 mm × 73 mm
CVD window	2.45 m	Thickness 50 µm	Diameter 20 mm
Focal plane	2.5 m	–	–

The cylindrical mirror length is 770 mm and a horizontal slot is incorporated in order to allow the higher-energy X-rays to pass. This horizontal slot can be made with a width of 5 mm along 150 mm of its initial length (for radiation emitted from the upstream dipole chamber) and 3 mm for the remainder of its length. Those apertures reduce the power and power density absorbed by the mirror to 2.1 W and 17 mW mm^{-2} for the upstream part and 15 mW and 0.2 mW mm^{-2} for the rest of the mirror.

The closest distances of the cylindrical mirror (downstream edge) and the cone-shaped mirror to the electron trajectory are 31.0 mm and 38.8 mm, respectively, which easily avoids impedance degradations.

Table 3 provides the optical properties (size, divergence, intensity) of the beam on the focal plane in the near-IR to the terahertz domain. Fig. 5 shows the corresponding ray-tracing simulation of the beam image and profiles focused at λ = 10 µm, where the Gaussian shapes indicate that the beam is almost aberration-free.

The beam emittance at this wavelength is 330 mm^2 mrad^2 (at 95% of the encircled energy) over a 150 mrad horizontal extraction aperture and represents a beam emittance improvement of over two orders of magnitude compared with existing IR beamlines that, up to now, do not take into account electron beam effects. Table 4 provides the mirrors' optical tolerances in order that the emittance is not degraded by more than 40%. By comparing these values with the current mechanical accuracies in the manufacture and alignment of dipole chambers (±500 µm and ±40 µrad) (Herbeaux, 2016), it is readily seen that thanks to this performant optical layout, which focuses independently the horizontal and vertical components of the BM source, IR beams with emittance degradations not exceeding 40% can be obtained from configurations using interdependent optimized optics and

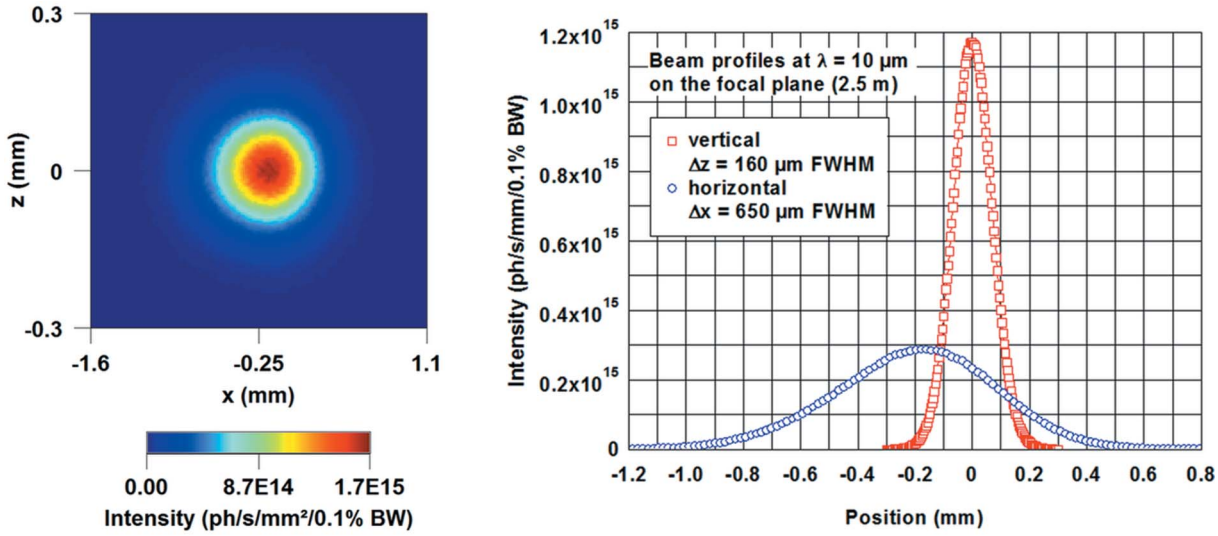

Figure 5
Ray-tracing simulation at λ = 10 µm, showing the photon beam image (left) and its horizontal and vertical projections (right) focused at 2.5 m from the source. The fully Gaussian shape of the focused beam indicates very low levels of aberrations.

Table 3
Optical beam properties at the focal plane in the near-IR to terahertz domain.

λ (µm)	FWHM size (H × V) (µm)	Divergence (H × V) (mrad @ 99%)	Flux [photons s^{-1} (0.1% bandwidth)$^{-1}$]
2	462 × 100	58.2 × 15.9	2.8×10^{14}
10	650 × 160	57.8 × 22.1	2.0×10^{14}
30	908 × 268	58.2 × 22.8	1.2×10^{14}
100	1513 × 538	58.4 × 22.8	5.3×10^{13}
1000	6142 × 2213	61.2 × 22.8	1.0×10^{13}

Table 4
Optics tolerances (at λ = 10 µm) based on limiting the beam emittance degradation to 40%.

Tolerances	Cylindrical mirror	Cone-shaped mirror
Pitch	±0.3 mrad	±2.8 mrad
Roll	±5.1 mrad	±1.9 mrad
Yaw	–	±1.9 mrad
Transverse translation	–	±0.9 mm
Longitudinal translation	±1.8 mm	±0.5 mm
Normal translation	±0.7 mm	±0.5 mm
$\Delta R/R$	±1.5%	±2.0%

dipole chambers, while providing brilliances of over two orders of magnitude higher than traditional IR beamlines.

4. Conclusion

In this paper, an IR optical layout removing the aberrations of BM sources (Moreno, 2015) is integrated inside a dipole chamber. This development brings an interesting solution in order to implement IR beamlines on space-restricted MBA lattices that would normally otherwise exclude this type of facility. The optical tolerances have been compared with the mechanical accuracies in the manufacture and alignment of the dipole chambers and show that the proposed solution is not only viable but, thanks to its optimized optical layout, can produce intense beams in the near- to mid-IR domain of two orders of magnitudes brighter compared with existing IR beamlines that do not take into account electron beam effects. Acquiring manufacturing expertise on this proposed solution should allow dipole chambers to provide almost aberration-free IR synchrotron endstations on current and ultimate storage rings.

Acknowledgements

The author thanks Paul Dumas and Ferenc Borondics for fruitful discussions concerning the technical aspects relating to the SMIS IR beamline. The author also thanks Christian Herbeaux, Keihan Tavakoli and José Dasilvacastro for helpful discussions and advice on the SOLEIL dipole chambers, at the root of the present paper, and for providing full three-dimensional schemes and technical drawings. The author also thanks Ryutaro Nagaoka for his expertise on the impedance and electron beam stability. Finally, the author thanks François Polack and James Ablett for engaging discussions about the optical and mechanical accuracies for project feasibility.

References

Bosch, R. A., May, T. E., Reininger, R. & Green, M. A. (1996). *Rev. Sci. Instrum.* **67**, 3346.
Carr, G. L., Dumas, P., Hirschmug, C. J. & Williams, G. P. (1998). *Nouv. Cim. D*, **20**, 375–395.
Chubar, O. & Elleaume, P. (1998). *Proceedings of the Sixth European Particle Accelerator Conference (EPAC'98)*, pp. 1177–1179.
Dumas, P., Jamin, N., Teillaud, J. L., Miller, L. M. & Beccard, B. (2004). *Faraday Discuss.* **126**, 289–302.
Dumas, P., Polack, F., Lagarde, B., Chubar, O., Giorgetta, J. L. & Lefrançois, S. (2006). *Infrared Phys. Technol.* **49**, 152–160.
Dumas, P. & Tobin, M. J. (2003). *Spectrosc. Eur.* **15**, 17–23.
Duncan, W. D. & Williams, G. P. (1983). *Appl. Opt.* **22**, 2914–2923.

Eriksson, M., Ahlbäck, J., Andersson, Å., Johansson, M., Kumbaro, D., Leemann, S. C., Lenngren, C., Lilja, P., Lindau, F., Lindgren, L.-J., Malmgren, L., Modeér, J., Nilsson, R., Sjöström, M., Tagger, J., Tavares, P. F., Thorin, S., Wallén, E., Werin, S., Anderberg, B. & Dallin, L. (2011). *Proceeding of the 2nd International Particle Accelerator Conference, IPAC2011*, San Sebastian, Spain, pp. 3026–3028.

Eriksson, M., Lindgren, L.-J., Sjöström, M., Wallén, E., Rivkin, L. & Streun, A. (2008). *Nucl. Instrum. Methods Phys. Res. A*, **587**, 221–226.

Herbeaux, C. (2016). Personal communication.

Howells, M. R. (1992). *Proceedings of the NATO Advanced Study Institute on New Directions in Research with Third-Generation Soft X-ray Synchrotron Radiation Sources*, Maratea, Italy, 28 June–10 July 1992, *NATO ASI Series E: Applied Sciences*, Vol. 254, p. 359. Dordrecht: Kluwer.

Kimura, S., Kimura, H., Takahashi, T., Fukui, K., Kondo, Y., Yoshimatsu, Y., Moriwaki, T., Nanba, T. & Ishikawa, T. (2001). *Nucl. Instrum. Methods Phys. Res. A*, **467–468**, 437–440.

Kimura, S., Nakamura, E., Imura, K., Hosaka, M., Takahashi, T. & Katoh, M. (2012). *J. Phys. Conf. Ser.* **359**, 012009.

Kirkpatrick, P. & Baez, A. V. (1948). *J. Opt. Soc. Am.* **38**, 766–774.

López-Delgado, R. & Szwarc, H. (1976). *Opt. Commun.* **19**, 286–291.

Moreno, T. (2015). *J. Synchrotron Rad.* **22**, 1163–1169.

Moreno, T. (2016). *J. Synchrotron Rad.* **23**, 1124–1130.

Moreno, T. & Idir, M. (2001). *J. Phys. IV Fr.* **11**, 527–531.

Moreno, T., Westfahl, H., Freitas, R. de O., Petroff, Y. & Dumas, P. (2013). *J. Phys. Conf. Ser.* **425**, 142003.

Nagaoka, R. (2004). *Proceedings of the Ninth European Particle Accelerator Conference, EPAC'04*, Lucerne, Switzerland, pp. 2041–2043.

Noda, H., Namioka, T. & Seya, M. (1974). *J. Opt. Soc. Am.* **64**, 1037–1042.

Roy, P., Guidi Cestelli, M., Nucara, A., Marcouille, O., Calvani, P., Giura, P., Paolone, A., Mathis, Y. L. & Gerschel, A. (2000). *Phys. Rev. Lett.* **84**, 483–486.

Schnell, M., Garcia-Etxarri, A., Huber, A. J., Crozier, K., Aizpurua, J. & Hillenbrand, R. (2009). *Nat. Photon.* **3**, 287.

Schweizer, E., Nagel, J., Braun, W., Lippert, E. & Bradshaw, A. M. (1985). *Nucl. Instrum. Methods Phys. Res. A*, **239**, 630–634.